Comparison of the absolute mass sensitivity of ring electrode QCM and standard QCM using electrodeposition

Jianguo Hu[a,b,*], Song Xue[c], Oliver Schneider[b], Göktug Yesilbas[b], Alois Knoll[b,*], Xianhe Huang[a,*]

[a] School of Automation Engineering, University of Electronic Science and Technology of China, Chengdu 611731, China
[b] Institut für Informatik VI, Technische Universität München, München 85748, Germany
[c] Physics of Energy Conversion and Storage, Technical University of Munich, Munich 85748, Germany

A B S T R A C T

In this work, we experimentally measured the absolute mass sensitivity of quartz crystal microbalance (QCM) resonators with one ring electrode on the sensing side and compared it to standard QCM resonators with disc electrodes on both sides using electrodeposition. This method allows to compare the absolute mass sensitivity of a ring electrode QCM and standard QCM resonators. The results showed that the average absolute mass sensitivity of a QCM resonator with a ring electrode on one side and a disc electrode on the other side is larger than the one of standard resonators with disc electrodes on both sides. If the ring electrode is facing the electrolyte, the absolute mass sensitivity is 10.28% higher, and for the disc electrode side it is still 5.33% higher. This shows that the ring electrode geometry improves the absolute mass sensitivity in comparison to a standard electrode structure, and therefore reveals a path to improve QCM detection sensitivity in electrochemical research.

1. Introduction

The quartz crystal microbalance (QCM) technique is of great importance for detecting small mass changes due to its ultrahigh mass sensitivity and simple structure [1-6]. The response of a QCM resonator to mass change is defined as QCM mass sensitivity, which is critical for practical applications. The common QCM resonators are typically made of a piezoelectric AT-cut quartz crystal disc patterned with two thin gold or aluminum film electrodes on both sides. A thickness shear mode (TSM) bulk acoustic wave is generated by applying an alternating voltage between the two electrodes [7]. Sauerbrey presented a relationship between the resonance frequency shift of the shear wave and the variation in interfacial mass [8],

$$\Delta f = f_R - f_0 = -\frac{2f_0^2}{\sqrt{\mu_q \rho_q}} \frac{\Delta m}{A},$$

(1)

where Δf is the resonance frequency shift due to surface mass loading; f_R and f_0 are the resonance frequencies of the quartz crystal with and without mass loading, respectively; Δm is the mass change on the QCM surface, A is the surface area of the deposit, μ_q is the shear modulus of AT-cut quartz crystal ($\mu_q = 2.947 \times 10^{11}$ g/cm·s²), and ρ_q is the density of quartz ($\rho_q = 2.643$ g/cm³). This equation indicates that the change of resonance frequency is always negative with the increase of surface

mass loading on the quartz.

According to Sauerbrey's equation and well known, the absolute mass sensitivity can be improved by reducing the thickness of the quartz crystal and thus increasing its fundamental resonance frequency f_0. However, it is quite difficult to fabricate and apply extremely thin quartz crystals because of their fragility. Common QCMs have a resonance frequency range of 5 to 10 MHz with a thickness between 167 and 330 μm [9]. Even though QCMs with a resonance frequency from 170 to 195 MHz have been realized by a special design, their reliability and durability are poor [10,11]. Considering these limitations, the improvement of the absolute mass sensitivity by optimizing the design of QCM electrode structure becomes attractive.

The QCM mass sensitivity is not uniform but follows a nearly Gaussian distribution [12,13]. A convincing example is that the frequency changes caused by the mass of particles deposited on different positions of the surface are not the same [14]. In fact, the mass sensitivity distribution is closely related to the particle displacement amplitude [15]. Richardson et al. presented a ring electrode design predicted by theory for sensitivity distribution to achieve a uniform mass sensitivity distribution [15]. Zhu et al. achieved a nearly uniform displacement distribution and mass sensitivity of the ring electrode quartz resonator by optimizing the size of the electrodes and the mass ratio of the electrode to the plate [16]. Shi et al. studied a quartz resonator with rectangular ring electrodes for getting a uniform vibration distribution

* Corresponding author at: School of Automation Engineering, University of Electronic Science and Technology of China, Chengdu 611731, China (J. Hu).
E-mail addresses: jianguo.hu@tum.de (J. Hu), knoll@mytum.de (A. Knoll), xianhehuang@uestc.edu.cn (X. Huang).

[17].

In this paper, we experimentally measured the absolute mass sensitivity of quartz crystal microbalance (QCM) resonators with one ring electrode on the sensing side and compared it to standard QCM resonators with disc electrodes on both sides using electrodeposition. This method allows to compare the absolute mass sensitivity of a ring electrode QCM and standard QCM resonators. We show that the average absolute mass sensitivity of a QCM resonator with a ring electrode on one side and a disc electrode on the other side is larger than the one of standard resonators with disc electrodes on both sides. This shows that the ring electrode geometry improves the absolute mass sensitivity in comparison to a standard electrode structure, and therefore reveals a path to improve QCM detection sensitivity for studying electrochemistry applications where a higher absolute mass sensitivity is desirable. These modified QCMs might also be beneficial for the study of viscoelastic layers, battery layers and reactions in ionic liquids where Sauerbrey's equation cannot be applied due to non-gravimetric contributions.

2. Experimental section

2.1. Specifications of ring electrode QCM and standard QCM

Modifying the design of the electrode structures is a central approach to achieving a higher absolute mass sensitivity for the fabrication of QCM sensors [18]. Recently, we designed a QCM resonator with one ring electrode on one side and a disc electrode on the other side

(Fig. 1) [19]. We showed that electrochemical QCM measurements are possible with that configuration, and determined the mass sensitivity constant S for both ring side or disc side of these resonators as working electrode (WE) [20]. In the current work, we compare the integral absolute mass sensitivity C as defined in Eq. (2) of such resonators with the one of resonators with a standard electrode (Fig. 1(b)) geometry (discs of equal area on both sides). Diameter (8.7 mm) and fundamental frequency (10 MHz) of the resonators were the same as in our earlier study [19]. The electrode thickness was 80 nm in all cases.

2.2. Calculations of absolute mass sensitivity based on electrodeposition

As before, we applied an electrodeposition approach to determine the QCM absolute mass sensitivity C. This method is actually often used in the experimental calibration and for verification of the theoretical values [21,22].

We experimentally determined the absolute mass sensitivity of QCMs with ring and disc electrodes by measuring the resonance frequency change of a quartz crystal during deposition of Cu from a sulfate based Cu(II) electrolyte and applying Faraday's laws of electrolysis. This electrolyte was selected, as sulfate based Cu(II) electrolytes had been used before for sensitivity analysis of QCM resonators and were recommended for calibration of such resonators [22-25]. Also, one of the authors had worked before with this electrolyte for QCM model studies [26]. Sulfate based electrolytes have the advantage that the standard potential for Cu(I)/Cu(0) is more positive than the one for Cu (II)/Cu(I), rendering Cu(I) unstable at Cu deposition potentials,
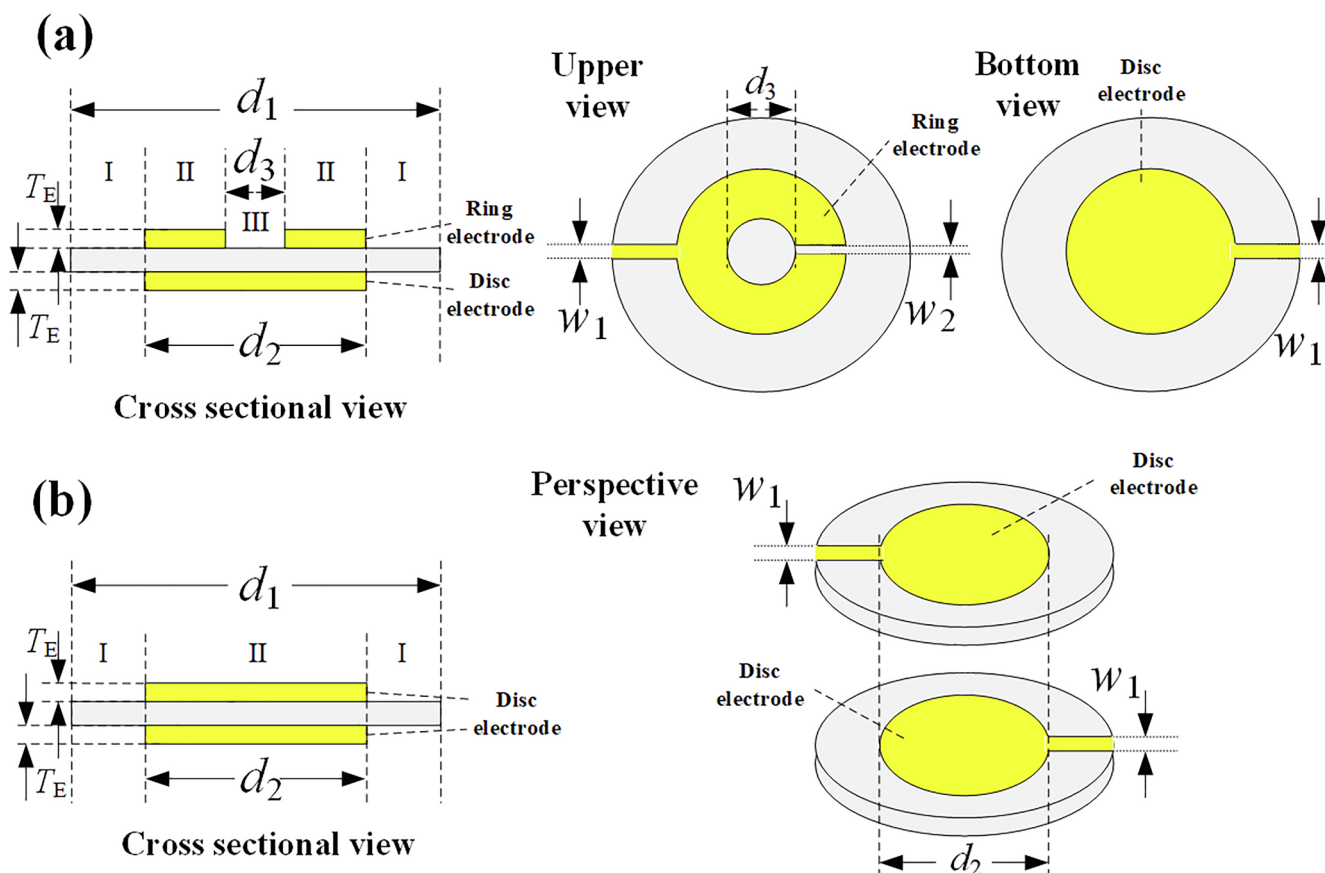

Fig. 1. Schematic drawings of the ring electrode and standard QCM resonators. (a) QCM resonators with a ring electrode on one side and a disc electrode on the other side; I, II: bare quartz surface or electrode layer on both sides, respectively; III: electrode layer on one side only; quartz diameter d_1 (d_1 = 8.7 mm), outer diameter of ring electrode d_2 (d_2 = 5.1 mm) and inner diameter of ring electrode d_3 (d_3 = 2 mm). W_1 (W_1 = 0.5 mm) and W_2 (W_2 = 0.3 mm) are the width of the electrode contact pads and an opening in the ring electrode (manufacturing restrictions), respectively. (b) Standard QCM resonators with two disc electrodes on both sides. d_1 (d_1 = 8.7 mm), d_2 (d_2 = 5.1 mm) are the quartz and the disc electrode diameter; I, II: bare quartz surface of electrode layer on both sides, respectively; W_1 (W_1 = 0.5 mm) is the width of the electrode contact pads. All electrodes have the thickness T_E (T_E = 800 Å).
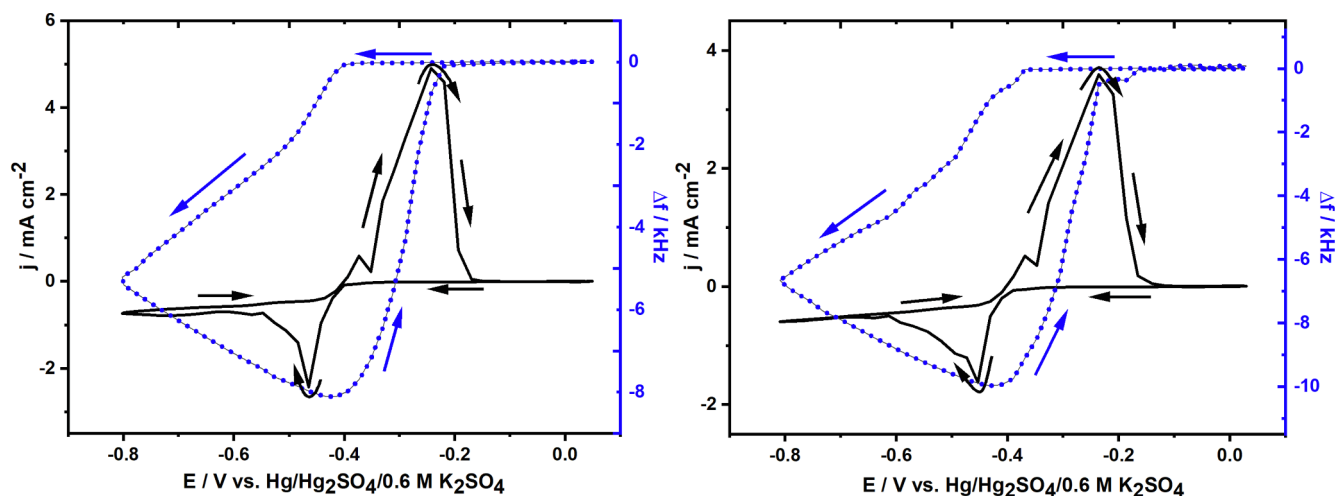
Fig. 2. Cyclic voltammograms of Cu deposition and dissolution in an electrolyte of 0.01 M CuSO$_4$·5H$_2$O, 0.1 M Na$_2$SO$_4$ and 5 mM H$_2$SO$_4$, at a sweep rate of 5 mV/s. Both current densities (lines) and related resonance frequency changes extracted from admittance spectra (blue dots). (a) Ring electrode, ring electrode QCM. (b) Disc electrode, standard QCM.

lowering the risk of loss of intermediate Cu(I) and eliminating Cu corrosion by Cu(II). Still, there is a slight chance that some Cu(I) may be lost due to diffusion away from the surface [27,28]. Oxide formation is avoided due to the low pH. A possible alternative would be based on Pb underpotential deposition [3,23,29,30]. However, the Cu electrolyte is less toxic and is based on bulk electrodeposition, causing larger frequency changes and therefore better signal to noise ration. Another alternative would have been silver deposition [31]. The calibration process can be summarized by [32],

$$C = \frac{\Delta f}{\Delta m} = \frac{df}{dm}, \tag{2}$$

$$m = \frac{QM}{zF}, \tag{3}$$

$$Q = \int_0^t Idt, \tag{4}$$

where Δf is the resonance frequency shift due to a surface mass loading; m is the electrodeposited Cu mass in grams, Q, F ($F = 96485$C/mol), M ($M = 63.5$ g/mol) and z are the total electric charge passing through the cell in coulombs, the Faraday constant, the molar mass of copper and the valency number of the Cu ions (i.e. $z = 2$), respectively. A larger value of C means that a given mass change causes a larger frequency change, i.e. a larger measurement signal and thus enhanced sensor sensitivity. I and t are the time-dependent copper deposition current and the total deposition time, respectively. Eq. (2) shows that the absolute mass sensitivity is determined by the resonance frequency shift caused by the mass changes on the electrode surface. Eqs. (3) and (4) are Faraday's laws of electrolysis and describe quantitative relationships between the amount of material produced at an electrode with the total conducted charge during an electrochemical reaction.

The electrochemical cell is the same as used in our earlier work [19]. The instrumental setup consisted of an Electrochemical Interface SI1287 (Solartron), a network analyzer (NA) E5100A from Agilent for measurement of the quartz admittance spectra, and a splitter box to connect the WE to both devices without causing interference. The electrolyte (100 ml) is made of 0.01 M CuSO$_4$·5H$_2$O, 0.1 M Na$_2$SO$_4$ and 5 mM H$_2$SO$_4$. The working electrode (WE) is the ring or disc electrode of the respective QCM resonator facing the side exposed to the electrolyte, while the electrode on the other side is insulated from the electrolyte via a sealing O-ring. It is mounted in a holder placed at the bottom of the cell. The counter electrode (CE) is a Pt wire, and the reference electrode (RE) is a commercial Hg/Hg$_2$SO$_4$/0.6 M K$_2$SO$_4$

electrode ($+0.658$ V vs. NHE), to which all potentials are referred to in this work. Experiments were carried out at room temperature (25 °C). The electrolyte was purged with Argon (Vol.99.999%, Westfalen AG, Germany) before and between the experiments. During the experiments, Ar bubbling through the electrolyte was stopped to avoid disturbing the experiment but above the electrolyte Ar purging was maintained. Cyclic voltammograms (CVs) were measured at a sweep rate of 5 mV/s and guided the selection of the deposition potential. Copper films were potentiostatically electrodeposited at -0.464 V on fifteen quartzes in total (group A: 5 quartzes with ring electrodes as upper and disc electrodes as back electrodes; group B: 5 quartzes with disc electrodes as upper and ring electrodes as back electrodes and group C: 5 quartzes with disc electrodes on both sides), in each case for 30 min.

2.3. Characterization of the thin films

To study the Cu film morphology, two symmetrical regions near the edge of the deposited films on all types of electrodes were characterized with atomic force microscopy (AFM). A multimode EC-STM/AFM instrument (Veeco Instrument, Inc.) with a Nanoscope IIID controller and the Nanoscope 5.31rl software (AFM tips, Bruker RTESP-300.) was used [33]. For each coating, two symmetric points close to the outer edge but on opposite sides of the Au working electrodes were selected for AFM measurements.

3. Results and discussion

3.1. Cyclic voltammograms and potentiostatic electrodeposition

The obtained voltammograms were in line with earlier work (cf. Fig. 2) [19]. Based on the CV data, a deposition potential of -0.464 V vs. Hg/ Hg$_2$SO$_4$/0.6 M K$_2$SO$_4$ was selected.

The Cu layers on the different electrodes were deposited potentiostatically for 30 min (Fig. 3). A typical Cottrell-like response with an initially rapid current decay followed by a more gradual decrease was observed. In the end, a small, relatively constant current was obtained, due to natural convection. The resonance frequency first showed as well a rapid decrease, corresponding to the initially larger currents, and then decreased linearly. The slopes of the Δf vs. T plot are then -3.102×10^4 Hz/s and -3.206×10^4 Hz/s for Fig. 4(a) and Fig. 4(b), respectively. Fig. 4 shows the relationship between the electric charge and the resonance frequency for the whole electrodeposition process. The Adj. R-Square values of linear fit lines are 0.99898 and
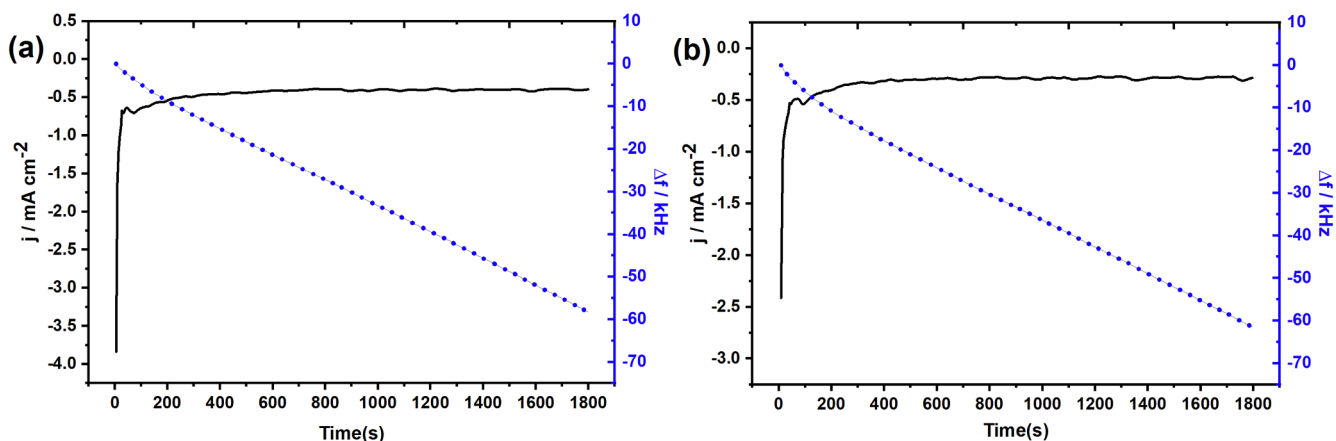
Fig. 3. Potentiostatic Cu electrodeposition at −0.464 V vs. Hg/Hg$_2$SO$_4$/0.6 M K$_2$SO$_4$ in deaerated 0.01 M CuSO$_4$·5H$_2$O, 0.1 M Na$_2$SO$_4$ and 5 mM H$_2$SO$_4$. (a) Ring electrode, ring electrode QCM. (b) Disc electrode, standard QCM.

0.9998, respectively. The $\Delta Q/A$ vs. Δf line in the experiment basically coincides with the straight line after linear fitting, which shows that the absolute mass sensitivity is basically unchanged throughout the whole deposition process, that is, the calculation is reliable.

3.2. Average roughness of the thin copper films

The average roughnesses at the two symmetrical measurement points were very close to each other for each coated quartz, e.g. for the disc electrode of a standard QCM resonator they are 19.32 nm and 21.65 nm, respectively. The roughness of the exemplary samples shown in Fig. 5(a), Fig. 5(b) and Fig. 5(c) are 18.80 nm, 22.32 nm and 19.32 nm, respectively. These AFM data indicated that all the measured regions exhibited a uniform morphology, and artifacts e.g. due to roughness effects in the QCM measurements are not to be expected. As Cu(I) formed as an intermediate during the Cu electrodeposition is thermodynamically unstable, Cu mental might also form by a disproportionation of Cu(I), i.e. an electrochemical-chemical mechanism. While this has no impact on the charge-mass-balance, it can affect the morphology of the layers observed in the ex-situ AFM images.

3.3. Absolute mass sensitivity of the ring QCM and standard QCM

After the deposition, the absolute mass sensitivities (Table 1) were calculated by Eqs. (2)–(4). A, C, $\overline{C}$, δ and R represent the surface area of the deposit, absolute mass sensitivity, average absolute mass sensitivity,

standard error and comparative relative indicators, respectively. The results shown for group A are for Cu films deposited on the ring electrodes and for group B on the disc electrodes of five (different) asymmetrical electrode QCM resonators each, all with the same specifications; group C represents results for Cu films deposited on the disc electrodes of five standard QCM resonators.

The minimum and maximum standard error are 4×10^7 Hz/g and 5×10^7 Hz/g, respectively, confirming the reliability of the approach. The average absolute mass sensitivities of group A, B and C are 1.1871×10^9 Hz/g, 1.1338×10^9 Hz/g and 1.0764×10^9 Hz/g, respectively. Totally, the R of group A is larger than that of group B, showing that the ring electrodes show an enhanced integral absolute mass sensitivity compared to the disc electrode. This is owed to the different electrode geometry. Additionally, the average absolute mass sensitivity of group B is greater than that of group C even though the WEs in this case have identical shape, thickness and surface area. These results show that the QCM resonators with an asymmetric electrode structure have an improved absolute mass sensitivity compared to the standard QCM even when the ring electrode serves "only" as the backside electrode. Please note that the region of the quartz oscillating is determined by the geometry of both electrodes, only regions with electrode contact on both sides are piezoelectrically active.

The comparative relative indicators of the average absolute mass sensitivity of the group A and B are 10.28% and 5.33% higher than those of the group C. It is known that a ring electrode QCM has an approximately uniform absolute mass sensitivity distribution, both from
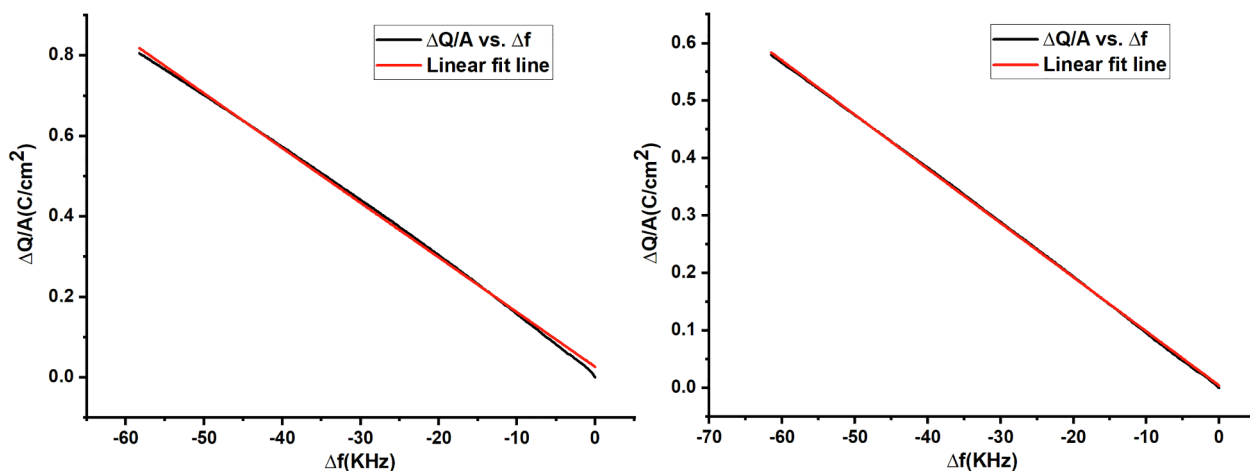

Fig. 4. Relationship between electric charge and resonance frequency in the whole electrodeposition process. The black line is the $\Delta Q/A$ vs. Δf relationship. The red line is a linear fit line based on $\Delta Q/A$ vs. Δf. (a) Ring electrode QCM. (b) Disc electrode of standard QCM.
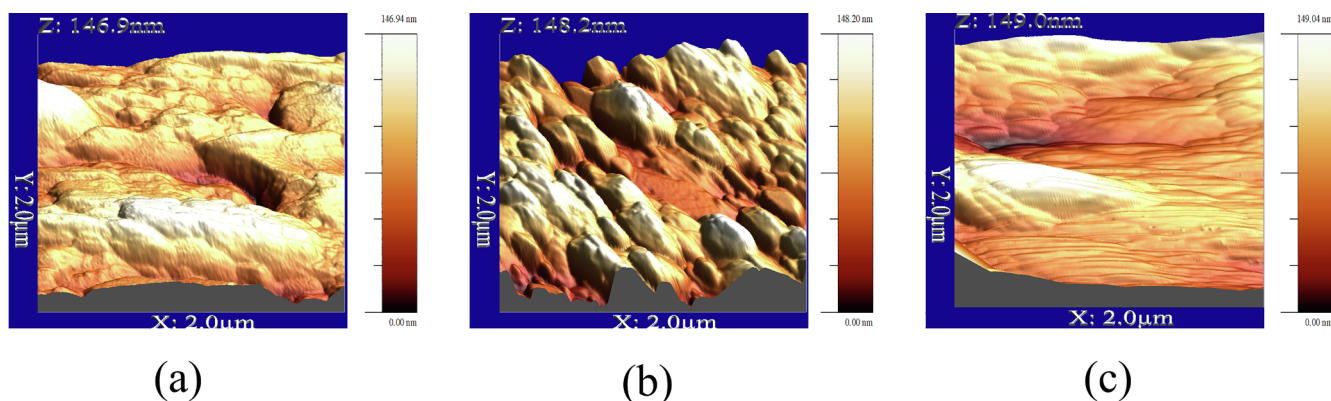
Fig. 5. Morphology of representative Cu films. (a) and (b) represent the ring and disc electrodes of the ring electrode QCM, respectively; (c) represents the disc electrode of the standard QCM.

Table 1
Comparison of the absolute mass sensitivity of ring QCM and standard QCM resonators.

Type	QCM-Ring	QCM-Disc	Standard QCM-Disc
$A(\text{cm}^2)$	0.190866	0.22228	0.222282
	1.28013	1.1181	1.06055
	1.14734	1.2407	1.07062
C (10^9 Hz/g)	1.21276	1.09889	1.15397
	1.12424	1.11401	1.06964
	1.17104	1.09753	1.02736
$\overline{C}$	1.187102	1.13385	1.076428
δ	0.05496	0.05404	0.041839
R	110.28%	105.33%	/

our own research [34] and from literature studies on the displacement of QCM resonators with ring-shaped electrodes [15-17]. This feature can contribute to the integrated absolute mass sensitivity and explain why for the disc electrode on an asymmetric QCM a larger sensitivity is obtained as compared to a disc electrode of the same size on a standard QCM resonator.

4. Conclusion

The calibration studies of QCM resonators with different electrode geometry in this communication show that the absolute mass sensitivity of QCM resonators with one ring electrode is improved compared to the absolute mass sensitivity of standard QCM resonators, and the absolute mass sensitivity of the ring electrodes is higher than those of the disc electrodes. The QCM with ring electrode reveals a path to improve QCM detection sensitivity for different applications where a higher absolute mass sensitivity is desirable.

Declaration of Competing Interest

The authors declare that they have no known competing financial interests or personal relationships that could have appeared to influence the work reported in this paper.

Acknowledgements

References

[1] Y. Ratieuville, P. Viers, J. Alexandre, G. Durand, A new electrochemical cell adapted to quartz crystal microbalance measurements, Electrochem. Commun. 2 (2000) 839–844.

[2] E.M. Pater, S. Bruckenstein, A.R. Hillman, Film mass and volume changes accompanying redox-driven solvent and salt transfer during redox switching of polyvinylferrocene films, J. Chem. Soc., Faraday Trans. 94 (1998) 1097–1103.

[3] O. Melroy, K. Kanazawa, J.G. Gordon II, D. Buttry, Direct determination of the mass of an underpotentially deposited monolayer of lead on gold, Langmuir 2 (1986) 697–700.

[4] L. Daikhin, E. Gileadi, G. Katz, V. Tsionsky, M. Urbakh, D. Zagidulin, Influence of roughness on the admittance of the quartz crystal microbalance immersed in liquids, Anal. Chem. 74 (2002) 554–561.

[5] V.E. Granstaff, S.J. Martin, Characterization of a thickness shear mode quartz resonator with multiple nonpiezoelectric layers, J. Appl. Phys. 75 (1994) 1319–1329.

[6] D.E. Diltemiz, R. Keçili, A. Ersöz, R. Say, Molecular imprinting technology in quartz crystal microbalance (QCM) sensors, Sensors 17 (2017) 454.

[7] D.W. Randolph, K.U. Anant, R.B. Venkat, High frequency thickness shear mode devices for organic vapor sensing, Sens. Actuat. B. 122 (2007) 635–643.

[8] G. Sauerbrey, Verwendung von Schwingquarzen zur Wägung dünner Schichten und zur Mikrowägung (Use of quartz vibration for weighing thin films on a microbalance), Z. Phys. 155 (1959) 206–222.

[9] P.T. Wang, J.W. Su, C.F. Su, W. Dai, G. Cernigliaro, H.W. Sun, An ultrasensitive quartz crystal microbalance-micropillars based sensor for humidity detection, J. Appl. Phys. 115 (2014) 224501.

[10] H. Ogi, H. Naga, Y. Fukunishi, M. Hirao, M. Nishiyama, 170-MHz electrodeless quartz crystal microbalance biosensor: capability and limitation of higher frequency measurement, Anal. Chem. 81 (2009) 8068–8073.

[11] A. Wessels, B. Klöckner, C. Siering, S.R. Waldvogel, Practical strategies for stable operation of HFF-QCM in continuous air flow, Sensors 13 (2013) 12012–12029.

[12] F. Josse, Y. Lee, S.J. Martin, R.W. Cernosek, Analysis of the radial dependence of mass sensitivity for modified-electrode quartz crystal resonators, Anal. Chem. 70 (1998) 237–247.

[13] J.Y. Gao, X.H. Huang, Y. Wang, The modified design of ring electrode quartz crystal resonator for uniform mass sensitivity distribution, IEEE Trans. Ultrason. Ferroelectr. Freq. Control 60 (2013) 2031–2034.

[14] J.R. Vig, A. Ballato, Comments about the effects of nonuniform mass loading on a quartz crystal microbalance, IEEE Trans. Ultrason. Ferroelectr. Freq. Control 45 (1998) 1123–1124.

[15] A. Richardson, V.R. Bhethanabotla, A.L. Smith, F. Josse, Patterned electrodes for thickness shear mode quartz resonators to achieve uniform mass sensitivity distribution, IEEE Sens. J. 9 (2009) 1772–1777.

[16] F. Zhu, B. Wang, X.Y. Dai, Z.H. Qian, I. Kuznetsova, V. Kolesov, B. Huang, Vibration optimization of an infinite circular AT-cut quartz resonator with ring electrodes, Appl. Mathem. Model. 72 (2019) 217–229.

[17] J.J. Shi, C.Y. Fan, M.H. Zhao, J.S. Yang, Thickness-shear vibration characteristics of an AT-cut quartz resonator with rectangular ring electrodes, Int. J. Appl. Electrom. Mech. 51 (2016) 1–10.

[18] P.T. Wang, J.W. Su, W. Dai, G. Cernigliaro, H.W. Sun, Ultrasensitive quartz crystal microbalance enabled by micropillar structure, Appl. Phys. Lett. 104 (2014) 043504.

[19] J.G. Hu, X.H. Huang, S. Xue, G. Yesilbas, A. Knoll, O. Schneider, Measurement of the mass sensitivity of QCM with ring electrodes using electrodeposition, Electrochem. Commun. 116 (2020) 106744.

[20] D. Johannsmann, The Quartz Crystal Microbalance in Soft Matter Research: Fundamentals and Modeling, Springer, Switzerland, 2015, p. 192.

[21] N. Shpigel, M.D. Levi, S. Sigalov, L. Daikhin, D. Aurbach, In situ real-time

mechanical and morphological characterization of electrodes for electrochemical energy storage and conversion by electrochemical quartz crystal microbalance with dissipation monitoring, Acc. Chem. Res. 51 (2018) 69–79.

[22] F.B. Li, A.R. Hillman, S.D. Lubetkin, D.J. Roberts, Electrochemical quartz crystal microbalance studies of potentiodynamic electrolysis of aqueous chloride solution: surface processes and evolution of H_2 and Cl_2 gas bubbles, J. Electroanal. Chem. 335 (1992) 345–362.

[23] D.A. Buttry, M.D. Ward, Measurement of interfacial processes at electrode surfaces with the electrochemical quartz crystal microbalance, Chem. Rev. 92 (1992) 1355–1379.

[24] M.D. Ward, E.J. Delawski, Radial mass sensitivity of the quartz crystal microbalance in liquid media, Anal. Chem. 63 (1991) 886–890.

[25] N. Casañ-Pastor, C. Zinck, C.R. Michel, E.M. Tejada-Rosales, G. Torres Gómez, Evidence of oxygen intercalation and mobility at room temperature in oxides: an electrochemical quartz microbalance study of intercalation in La_2CuO_4, Chem. Mater. 13 (2001) 2118–2126.

[26] O. Schneider, S. Matić, C. Argirusis, Application of the electrochemical quartz crystal microbalance technique to copper sonoelectrochemistry Part 1. sulfate-based electrolytes, Electrochim. Acta 53 (2008) 5485–5495.

[27] E. Gileadi, V. Tsionsky, Studies of electroplating using an EQCM. I. Copper and silver on gold, J. Electrochem. Soc. 147 (2000) 567–574.

[28] V. Tsionsky, E. Gileadi, Early stages in the electroplating of copper and silver on gold, Mater. Sci. Eng., A 302 (2001) 120–127.

[29] M. Hepel, S. Bruckenstein, Tracking anion expulsion during underpotential deposition of lead at silver using the quartz microbalance, Electrochim. Acta 34 (1989) 1499–1504.

[30] M. Hepel, K. Kanige, S. Bruckenstein, Expulsion of borate ions from the silver/solution interfacial region during underpotential deposition discharge of Pb(II) in borate buffers, Langmuir (6) (1990) 1063–1067.

[31] S. Bruckenstein, B. Miller, Circuit for tansient-free current-potential control conversion, J. Electrochem. Soc. 117 (1970) 1040–1044.

[32] D.R. Gabe, Coulometric techniques for surface coatings, Trans. IMF 77 (1999) 213–217.

[33] I. Horcas, R. Fernández, J.M. Gómez-Rodríguez, J. Colchero, J. Gómez-Herrero, A.M. Baro, WSXM: a software for scanning probe microscopy and a tool for nanotechnology, Rev. Sci. Instrum. 78 (2007) 013705.

[34] X.H. Huang, Q.S. Bai, P. Wei, J.G. Hu, Quartz crystal microbalance with approximately uniform sensitivity distribution, Anal. Chem. 90 (2018) 6367–6370.